ADVANCED FUNCTIONAL MATERIALS
www.afm-journal.de

2D Dual-Metal Zeolitic-Imidazolate-Framework-(ZIF)-Derived Bifunctional Air Electrodes with Ultrahigh Electrochemical Properties for Rechargeable Zinc–Air Batteries

Tingting Wang, Zongkui Kou, Shichun Mu, Jingping Liu, Daping He, Ibrahim Saana Amiinu, Wen Meng, Kui Zhou, Zhixiong Luo, Somboon Chaemchuen, and Francis Verpoort**

Here first a 2D dual-metal (Co/Zn) and leaf-like zeolitic imidazolate framework (ZIF-L)-pyrolysis approach is reported for the low-cost and facile preparation of Co nanoparticles encapsulated into nitrogen-doped carbon nanotubes (Co-N-CNTs). Importantly, the reasonable Co/Zn molar ratio in the ZIF-L is the key to the emergence of the encapsulated microstructure. Specifically, high-dispersed cobalt nanoparticles are fully encapsulated in the tips of N-CNTs, leading to the full formation of highly active Co–N–C moieties for oxygen reduction and evolution reactions (ORR and OER). As a result, the obtained Co-N-CNTs present superior electrocatalytic activity and stability toward ORR and OER over the commercial Pt/C and IrO_2 as well as most reported metal-organic-framework-derived catalysts, respectively. Remarkably, as bifunctional air electrodes of the Zn–air battery, it also shows extraordinary charge–discharge performance. The present concept will provide a guideline for screening novel 2D metal-organic frameworks as precursors to synthesize advanced multifunctional nanomaterials for cross-cutting applications.

1. Introduction

To maximally transform current fossil fuel-based economy into future renewable energy economy, the dominant lithium-ion batteries should be gradually replaced by new energy-storage devices due to numerous safety incidents and obstacles,[1] including transportation restrictions, limited lithium supply, high cost, and insufficient energy density.[2] Over the past few decades, benefiting from a higher theoretical energy density, low cost, and high security, rechargeable metal–air batteries have attracted renewed interest as a possible energy-storage solution.[3]

Zn is the fourth most earth-abundant metal and could sustain large battery production to meet the growing demand of the global electrical vehicle industry. Zn–air batteries have been suggested to be a promising metal–air system for practical use.[4–7] The lack of stable and effective bifunctional air electrodes is one of the main challenges for Zn–air battery technology. Although precious metals such as Pt, Ir, Ru, etc., have been used as high-active electrocatalysts for oxygen reduction and evolution reactions (ORR and OER), respectively, their high cost and poor stability are hampering commercialization of Zn–air batteries.[8]

Recently, transition metal nanoparticles encapsulated into graphene layers or carbon nanotubes have been observed to present extraordinary activity and stability for ORR and OER.[9–11] The surface carbon layer in the encapsulation structure not only prevents oxidation and aggregation of transition metal nanoparticles in the electrocatalytic process[12,13] but also captures electrons from metal nanoparticles.[9,14] In addition, the doping of nitrogen into carbon lattices can further promote the electron transfer to the adjacent carbon atoms.[15,16] Such a synergetic effect stimulates an excellent electrocatalytic activity and stability on carbon shells.[17,18] However, the low-cost and facile synthetic

T. T. Wang, Dr. Z. K. Kou, Prof. S. C. Mu, Prof. J. P. Liu, Prof. D. P. He, Dr. I. S. Amiinu, W. Meng, Dr. K. Zhou, Z. X. Luo, Dr. S. Chaemchuen, Prof. F. Verpoort
State Key Laboratory of Advanced Technology for Materials Synthesis and Processing
Wuhan University of Technology
Wuhan 430070, P. R. China
E-mail: msc@whut.edu.cn; Francis.verpoort@ugent.be
Prof. J. P. Liu, W. Meng, Z. X. Luo, Prof. F. Verpoort
School of Chemistry
Chemical Engineering and Life Sciences
Wuhan University of Technology
Wuhan 430070, P. R. China
Prof. D. P. He
Hubei Engineering Research Center of RF-Microwave Technology and Application
Wuhan University of Technology
Wuhan 430070, P. R. China
Prof. F. Verpoort
National Research Tomsk Polytechnic University
Lenin Avenue 30, 634050 Tomsk, Russian Federation
Prof. F. Verpoort
Ghent University
Global Campus Songdo, 119 Songdomunhwa-Ro
Yeonsu-Gu, Incheon, Korea

The ORCID identification number(s) for the author(s) of this article can be found under https://doi.org/10.1002/adfm.201705048.

DOI: 10.1002/adfm.201705048

 © 2017 WILEY-VCH Verlag GmbH & Co. KGaA, Weinheim

method for high-dispersed transition metal nanoparticles encapsulated within nitrogen-doped carbon is still an open issue.

Very recently, metal-organic frameworks (MOFs), particularly zeolitic imidazolate frameworks (ZIFs), have been used as solid-phase precursors to prepare multifunctional carbon nanomaterials because of low cost, high yield, and nitrogen self-doping.[19–21] Their 2D counterparts may be good candidates as precursors due to large surface area and high accessible active sites. Nevertheless, 2D ZIFs have received far less attention. Here, we report a dual-metal (Co/Zn) leaf-like ZIF-pyrolysis approach for the scalable preparation of Co nanoparticles encapsulated into nitrogen-doped carbon nanotubes (Co-N-CNTs). High-angle annular dark field-scanning transmission electron microscopy (HAADF-STEM) coupled with X-ray photoelectron spectroscopy (XPS) is conducted to disclose the symbiotic relationship between N and Co nanoparticles across the tips of CNTs which can result in full formation and usage of highly active Co–N–C moieties. As a result, the resultant Co-N-CNTs have been demonstrated to be the excellent bifunctional air electrodes. To expand them to the practical applications, we developed primary and rechargeable Zn–air batteries with significantly reduced ORR and OER overpotentials, and thus a high current density of ≈90 mA cm^{-2}, a high peak power density of ≈101 mW cm^{-2}, as well as good stability (130 cycles for 15 h of operation).

2. Results

2.1. Electrocatalyst Preparation and Characterizations

As preferred precursors, the novel zeolitic imidazolate frameworks with 2D leaf-like microstructure (ZIF-L) are simply synthesized by mixing a given amount of $Zn(NO_3)_2 \cdot 6H_2O$ and $Co(NO_3)_2 \cdot 6H_2O$ with 2-methylimidazole (2-mIm) at room temperature for 3 h (**Figure 1**a; Table S1, Supporting Information).[22] Figure 1b shows a typical photograph of the 80 mL scale synthetic process toward the representative Co/Zn (1:1) ZIF-L containing abundant Co, N, and C atoms, and the resultant is investigated by powder X-ray diffraction pattern (PXRD) and various resolution scanning electron microscope (SEM) analyses (Figure S1, Supporting Information). The leaf-shaped morphology of Co/Zn (1:1) ZIF-L can be observed (Figure 1c). Subsequently, the Co-N-CNTs are obtained by a straightforward pyrolysis of Co/Zn (1:1) ZIF-L at 900 °C for 2 h in an Ar atmosphere. The hierarchical networks are composed of interconnected CNTs (Figure 1d). The microstructure is also investigated by transmission electron microscopy (TEM; Figure 1e–g and Figure S2a in the Supporting Information). Figure 1e confirms Co nanoparticles encapsulated in a shell consisted of CNTs with several hundred nanometers in length. Furthermore, a high-resolution TEM (HR-TEM) image reveals that these thick multiwalled CNTs and Co nanoparticles are crystalline and the lattice fringes with an interplanar distance of ≈3.7 and ≈2.05 Å correspond to the C (002) and β-Co (111) facets,[9] respectively (Figure 1f; Figure S2b, Supporting Information). It is interesting that nitrogen only coexist with cobalt across the tips of CNTs (Figure 1g; Figure S3, Supporting Information). Thus, abundant Co–N–C moieties as active sites[23,24] are fully exposed on the surface of CNTs, which would be beneficial to the enhanced electrocatalytic properties.

Importantly, metal species in the precursor is crucial in obtaining encapsulated microstructure. By choosing pure Zn ZIF-L or Co ZIF-L as precursors (their leaf-shaped morphology and chemical phase have also been investigated by PXRD and SEM images; Figures S4 and S5, Supporting Information), it can be seen that the derived resultants present different morphology from Co-N-CNTs (Figures S6 and S7, Supporting Information). For pure Zn ZIF-L, the final product consists of nitrogen-doped carbon nanoribbon networks (N-CNRs; Figure S6, Supporting Information); when using pure Co ZIF-L as precursors, the final product consists of Co nanoparticle supported nitrogen-doped carbon nanosheets (Co/N-CNSs; Figure S7, Supporting Information).

The crystalline nature of the above-mentioned carbon materials in the networks is further confirmed by PXRD patterns (**Figure 2**a). The peak at about 22.8° corresponds to the C (002) plane.[21] For the resultant Co-N-CNTs and Co/N-CNSs, the additional peaks at about 44.3° are attributed to metallic β-Co (PDF #15-0806),[9] consistent with the HR-TEM results. Raman spectra of the products (Figure 2b) also reveal the characteristic G and D bands of carbon, which are related to the graphitic sp^2-carbon and disordered or defect carbon, respectively.[25] Two peaks. Two peaks centered at ≈471 and ≈675 cm^{-1} in the Raman spectrum of Co/N-CNSs are assigned to metallic Co.[22] For Co-N-CNTs, the absence of metallic Co spectrum indicates that Co nanoparticles can be fully encapsulated in multiwalled CNTs with ≈4 nm thickness (Figure 1f) which is beyond the depth of Raman spectroscopy detection (≈2 nm).[26]

The chemical composition and the effect of N doping are investigated by XPS (Figure S8a, Supporting Information). The high-resolution C 1s spectrum can be deconvolved into two main bands, corresponding to C—C at ≈284.7 eV[27] and C=N at ≈285.6 eV[27] (Figure S9a–c, Supporting Information). The high-resolution N 1s spectra for Co-N-CNTs and Co/N-CNSs reveal the presence of two types of nitrogen species, Co-N_x at ≈399.0 eV[28] and graphitic N at ≈401.3 eV[29] (Figure 2c), which is more beneficial for increasing catalytic performance than that of pyridinic N and pyrrolic N, respectively. The atomic percentage of N dopant is about 3.86 at% for the Co-N-CNTs (Figure S8b, Supporting Information). For N-CNRs, the absence of metallic Co leads to the presence of another two types of nitrogen species, pyridinic N at ≈398.4 eV and pyrrolic N at ≈400.7 eV[30] (Figure 2c). The Co 2p spectrum in the Co-N-CNTs exhibits two prominent bands at 779.9 and 795.7 eV, assigned to Co $2p_{3/2}$ and Co $2p_{1/2}$,[31] respectively (Figure S9d, Supporting Information). On the basis of inductively coupled plasma (ICP), the content of the Co species increases linearly with more cobalt nitrate added to precursors, but Zn species fully disappear after pyrolysis of the precursors (Figure S10, Supporting Information) because of the lower vaporization temperature (800 °C) of metallic Zn.[32]

N_2 sorption isotherms of Co-N-CNTs can be identified as type-IV isotherms, with a pronounced hysteresis loop, suggesting the existence of a mesoporous structure[33] (Figure 2d). Moreover, the Co-N-CNT sample shows a relatively broad pore distribution with an average pore size of ≈3.8 nm (Figure 2e). The specific surface area estimated by the Brunauer–Emmett–Teller (BET) method and the total pore volume are 250 m^2 g^{-1} and 0.24 cm^3 g^{-1}, respectively.

© 2017 WILEY-VCH Verlag GmbH & Co. KGaA, Weinheim

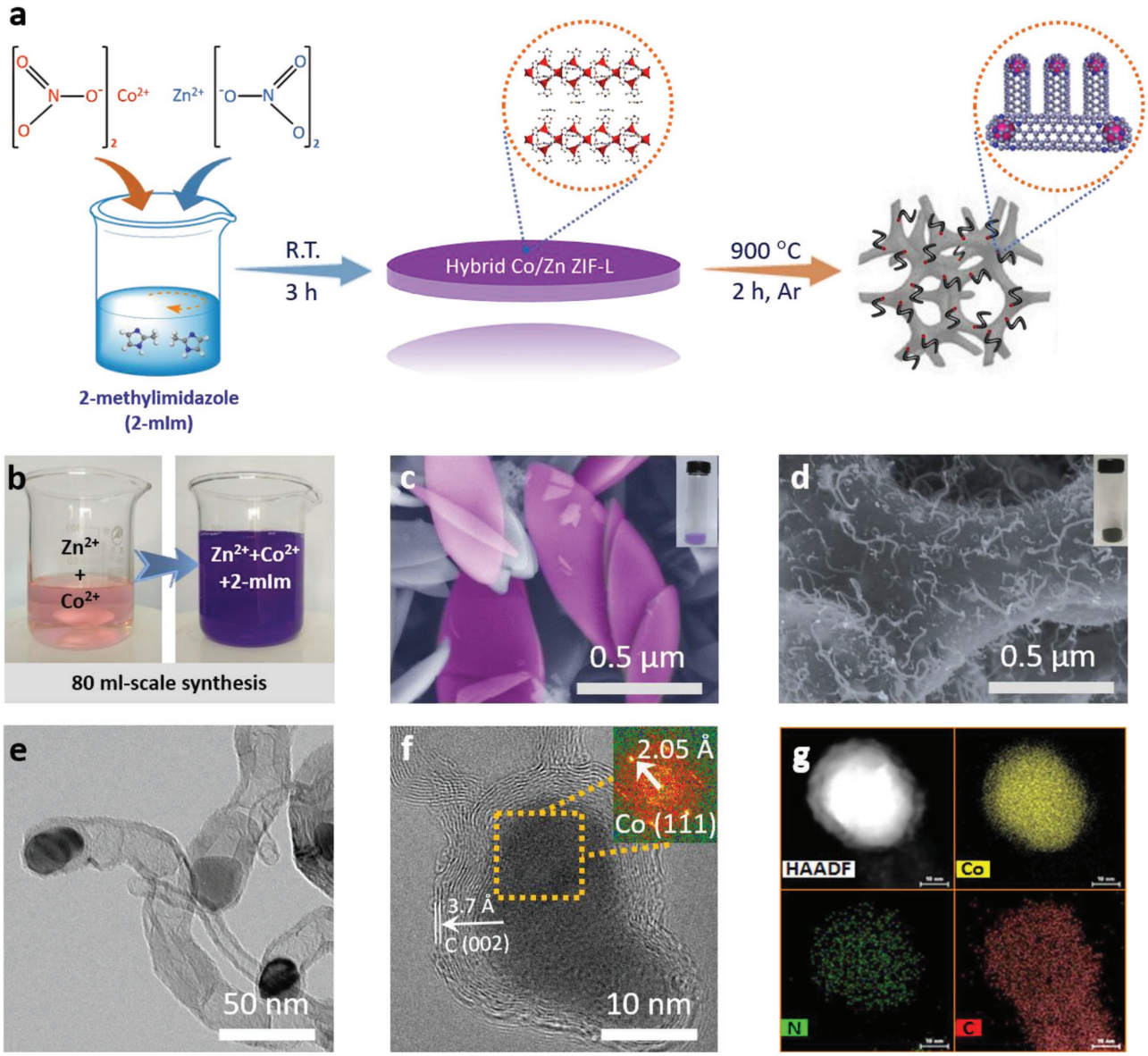

Figure 1. Preparation and electron microscopy characterization of hybrid Co/Zn ZIF-L and Co-N-CNTs. a) Schematic illustration toward the synthetic process of Co-N-CNTs. b) Photographs of 80 mL scale synthesis. SEM images of c) Co/Zn (1:1) hybrid ZIF-L and d) its resultant Co-N-CNTs. The inset images show the corresponding photographs of as-prepared powders. e) TEM and f) high-resolution TEM images of Co-N-CNTs. The corresponding Fourier transformed image can be seen in the inset image. g) HAADF-STEM image and the corresponding EDS mapping of hybrid Co/Zn (1:1) ZIF-L-derived Co-N-CNTs, showing that N follows with Co in the CNT networks.

To better understand the formation and evolution of Co-N-CNTs, 2D ZIF-L sheets with different molar ratios of Co and Zn pyrolyzed under the same conditions are further investigated (Figure S11–S13, Supporting Information). At a lower Co/Zn molar ratio of 1:2, the surface of the framework shows a few short CNTs as well as enlarged Co nanoparticles (**Figure 3**a,b; Figure S12, Supporting Information), which are mainly attributed to the insufficient limiting force of Zn and insufficient growth of CNTs.[32] With the increase of molar ratio to 2:1, more Co amount allows the formation of more CNTs while the size of Co particles becomes much bigger[18] (Figure 3c,d; Figure S13, Supporting Information). The microstructure of the resultant is therefore remarkably different from Co-N-CNT frameworks. Therefore, the current approach offers a versatile strategy for the controlled design and synthesis of 2D ZIF-derived metal nanoparticles encapsulated into carbon nanomaterials considering the large variety of 2D ZIF flakes available.

2.2. Electrochemical Evaluation of Co-N-CNTs for ORR and OER

The Co nanoparticles encapsulated into N-doped carbon nanotubes microstructure make the Co-N-CNTs attractive as nonnoble metal-based electrocatalysts.[34] To evaluate the electrocatalytic performance of the Co-N-CNTs, we performed

© 2017 WILEY-VCH Verlag GmbH & Co. KGaA, Weinheim

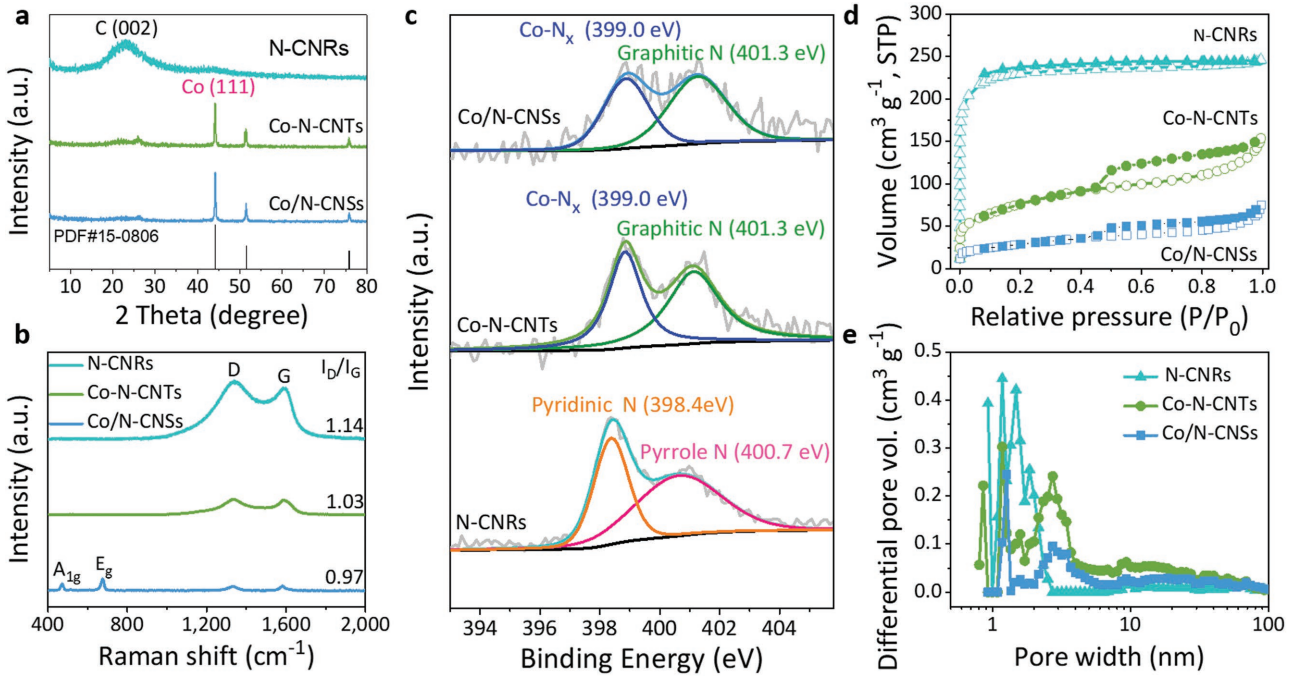

Figure 2. Chemical phase, surface chemical state, and pore structure of Zn ZIF-L-derived N-doped carbon nanoribbons (N-CNRs), hybrid Co/Zn (1:1) ZIF-L-derived Co-N-CNTs and Co ZIF-L-derived Co nanoparticles supported on the N-doped carbon nanosheets (Co/N-CNSs). a) X-ray diffraction patterns. b) Raman spectra. c) Curve-fitted high-resolution N 1s XPS spectra. d) N_2 adsorption–desorption isotherms and e) the corresponding pore size distribution curves.

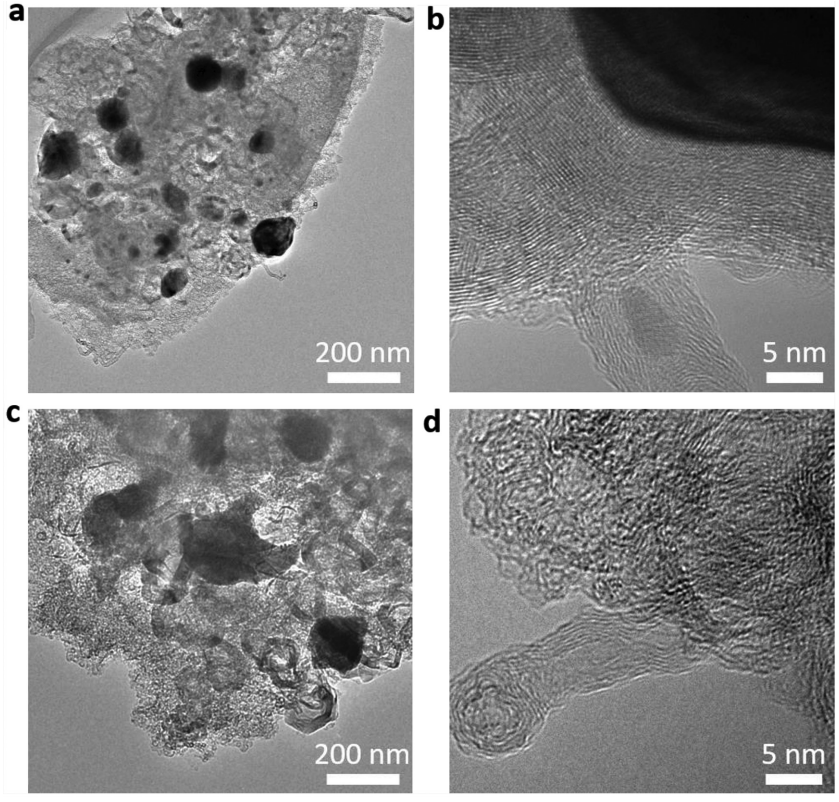

Figure 3. Morphology and structural characterization of 2D ZIF-L-derived composites. a) TEM and b) HR-TEM images of the product derived from Co/Zn (1:2) ZIF-L flakes. c) TEM and d) HR-TEM images of the product derived from Co/Zn (2:1) ZIF-L flakes.

linear sweep voltammetry (LSV) measurements at different rotating rates in 0.1 M KOH solution. **Figure 4**a reproduces the LSV curves measured on a rotating disk electrode (RDE) at a rotating speed of 1600 rpm in an aqueous solution of 0.1 M KOH, with a more positive onset potential ($E_{onset} \approx 0.97$ V vs reversible hydrogen electrode, RHE) along with a higher half-wave potential ($E_{1/2} \approx 0.90$ V) for Co-N-CNTs than that of Pt/C ($E_{1/2} \approx 0.87$ V), N-CNRs ($E_{1/2} \approx 0.78$ V), and Co/N-CNTs ($E_{1/2} \approx 0.72$ V).

For the catalysts derived from various ZIF-L with different Co/Zn molar ratios, the E_{onset} and $E_{1/2}$ obtained from the corresponding LSV plots are summarized in Figure S14 (Supporting Information). On the one hand, although the Co/Zn (2:1) ZIF-L has the highest Co content (Figure S13, Supporting Information), the relatively low Zn content could not be conducive to the encapsulating microstructure due to the formation of the larger Co nanoparticles (Figure 3c) and hence a relatively poor electrocatalytic activity was observed. On the other hand, although the encapsulating microstructure remained by increasing the Zn content, the relatively low Co content for Co/Zn (1:2) ZIF-L would be insufficient to catalyze the formation of the perfect CNT frameworks

© 2017 WILEY-VCH Verlag GmbH & Co. KGaA, Weinheim

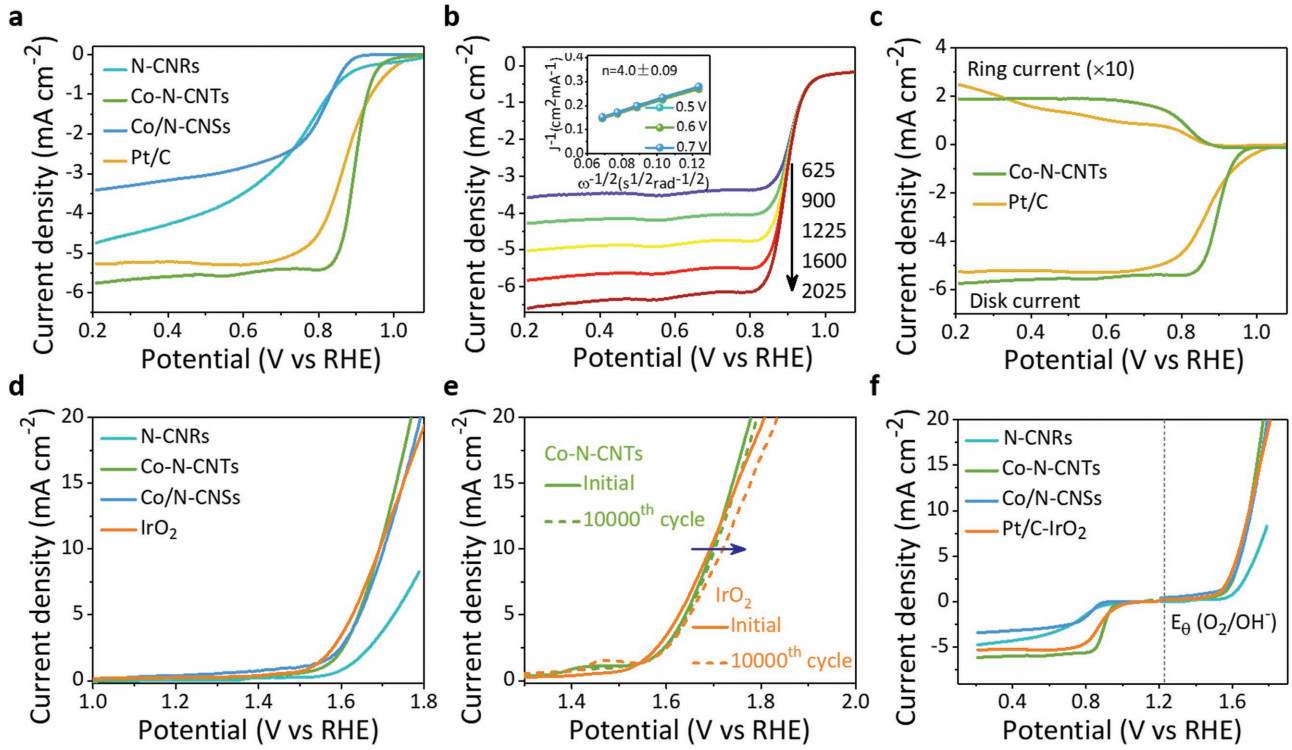

Figure 4. ORR and OER performance of the final products. a) LSV curves of different catalysts for ORR in O_2-saturated 0.1 M KOH at 1600 rpm. b) LSV curves of the optimal Co-N-CNT catalyst for ORR at various rotating speeds, and the inset represents the corresponding K–L plots at different potentials including the calculated number of electron transfer (n) per O_2. c) LSV curves of Co-N-CNTs and Pt/C (the inset image) before and after i–t chronoamperometric response at 0.9 V versus RHE for 20 000 s. d) LSV curves of different catalysts for OER at 1600 rpm in O_2-saturated 0.1 M KOH. e) LSV curves of Co-N-CNTs and IrO_2 before and after 10 000 potential cycles at a potential range of 1.4–1.8 V versus RHE and a sweep speed of 50 mV s^{-1}. f) LSV curves of different catalysts for both ORR and OER in O_2-saturated 0.1 M KOH at 1600 rpm. For all LSV curves, the scan rate is 5 mV s^{-1}. The catalyst loading is 0.81 mg cm^{-2} for all catalysts except Pt/C (20 μg_{Pt} cm^{-2}) and IrO_2 (0.1 mg cm^{-2}).

(Figure 3a; Figure S12, Supporting Information), resulting in a reduction in the active sites and the electrocatalytic activity. These results indicate that Co-N-CNTs obtained from Co/Zn (1:1) ZIF-L are the best ORR electrocatalysts and even better than Pt/C, highlighting the importance of the Co-N-CNT networks for ORR.

The electron transfer number per oxygen molecule (n) for ORR was determined from the LSV curves (Figure 4b; Figure S15, Supporting Information) according to the Koutechy–Levich (K–L) equation (for details see the Supporting Information). The K–L plots (the inset image of Figure 4b) show linear relationships between j_k^{-1} and $\omega^{-1/2}$ (where j_k is the kinetic current and ω is the electrode rotating rate), with a similar slope for the Co-N-CNT and Pt/C electrodes, from which n was determined to be ≈4.0, suggesting a preferable four-electron pathway for ORR.[35]

To further evaluate the ORR pathways for the catalyst investigated in this study, we performed rotating ring-disk electrode (RRDE) measurements. As shown in Figure 4c, Co-N-CNTs exhibited higher disk current densities (≈6 mA cm^{-2}) for O_2 reduction and lower ring current densities (≈0.018 mA cm^{-2}) for peroxide oxidation than those of Pt/C. Notably, the disk current could be decreased significantly for the catalysts derived from different precursors (Figure S16, Supporting Information). Figure S17a (Supporting Information) shows the percentage of peroxide species with respect to the total oxygen reduction products, and Figure S17b (Supporting Information) shows the electron transfer numbers calculated from the RRDE curves (for details see the Supporting Information). It can be envisioned that oxygen molecules were reduced to water via a nearly four-electron pathway (n is over 3.95) with a small ratio of peroxide species (less than 3%), in agreement with the results from the K–L plots. In comparison with the Pt/C catalyst, the Co-N-CNT electrode also exhibits a better long-term stability, higher resistance to the methanol crossover effect and CO poisoning effect (Figure S18, Supporting Information) in oxygen-saturated 0.1 M KOH, and comparable catalytic activity and stability, even in an acidic electrolyte (Figures S19–S21, Supporting Information). Moreover, the encapsulated microstructure of Co-N-CNTs is almost unchanged by long-term electrocatalytic process (Figure S22, Supporting Information). These results strongly demonstrate that our Co-N-CNTs is a superior ORR electrocatalyst.

The OER catalytic activities of the Co-N-CNTs and commercial IrO_2 were also investigated by LSV curves obtained on RDE at 1600 rpm. As shown in Figure 4d, the Co-N-CNTs present a lower overpotential (1.69 V) to collect a high catalytic current density of 10 mA cm^{-2} compared to the commercial IrO_2 and Co/N-CNSs as well as N-CNRs. Meanwhile, the Co-N-CNT electrode displays a lower overpotential drop than that of IrO_2

© 2017 WILEY-VCH Verlag GmbH & Co. KGaA, Weinheim

when suffering from 10 000 potential cycles (Figure 4e), indicating an excellent stability. The reversible oxygen electrode property can be evaluated by the variance of OER and ORR metrics ($\Delta E = E_{j=10} - E_{1/2}$, where $E_{j=10}$ is the operating potential at 10 mA cm^{-2} in OER and $E_{1/2}$ is the half-wave potential in ORR). The smaller ΔE represents a superior reversible oxygen electrode.[8,36] As shown in Figure 4f, the Co-N-CNTs exhibit a small ΔE value of 0.79 V, which largely surpassed noble metal benchmarks (e.g. Pt/C–IrO_2 hybrid catalysts in this work, ΔE = 0.83 V) and the highly active bifunctional catalysts (NiCo/PFC,[37] ΔE = 0.84 V; Co_3O_4/NPGC,[38] ΔE = 0.84 V; N-GCNT/$FeCo^3$, ΔE = 0.81 V). A wider comparison of high-performance bifunctional catalysts with various chemical phases and different electrode microstructures further verifies that Co-N-CNTs is one of the state-of-the-art bifunctional catalysts reported so far (see detailed comparison in Table S2 in the Supporting Information).

2.3. Co-N-CNTs as Air Cathodes in Primary and Rechargeable Zn–Air Batteries

Bifunctional catalysts for both ORR and OER are highly desirable for use in Zn–air battery applications. To this end, we explored the possibility of using our Co-N-CNTs as bifunctional air electrodes of Zn–air batteries (Figure S23, Supporting Information). The initial voltage efficiency of this two-electrode rechargeable Zn–air battery is 61.1% at current densities of 2 mA cm^{-2} (**Figure 5**a). As shown in Figure 5b, The Co-N-CNT electrode shows a current density of ≈90 mA cm^{-2} and a peak power density of ≈101 mW cm^{-2} over those of a Pt/C–IrO_2 (1:1) hybrid catalyst (≈80 mA cm^{-2} and 75 mW cm^{-2}). Such good performances of our Co-N-CNT frameworks derive from their large BET area and mesoporous structure (Figure S24, Supporting Information) as well as high-density encapsulated microstructure, which facilitates efficient diffusion of O_2 gas

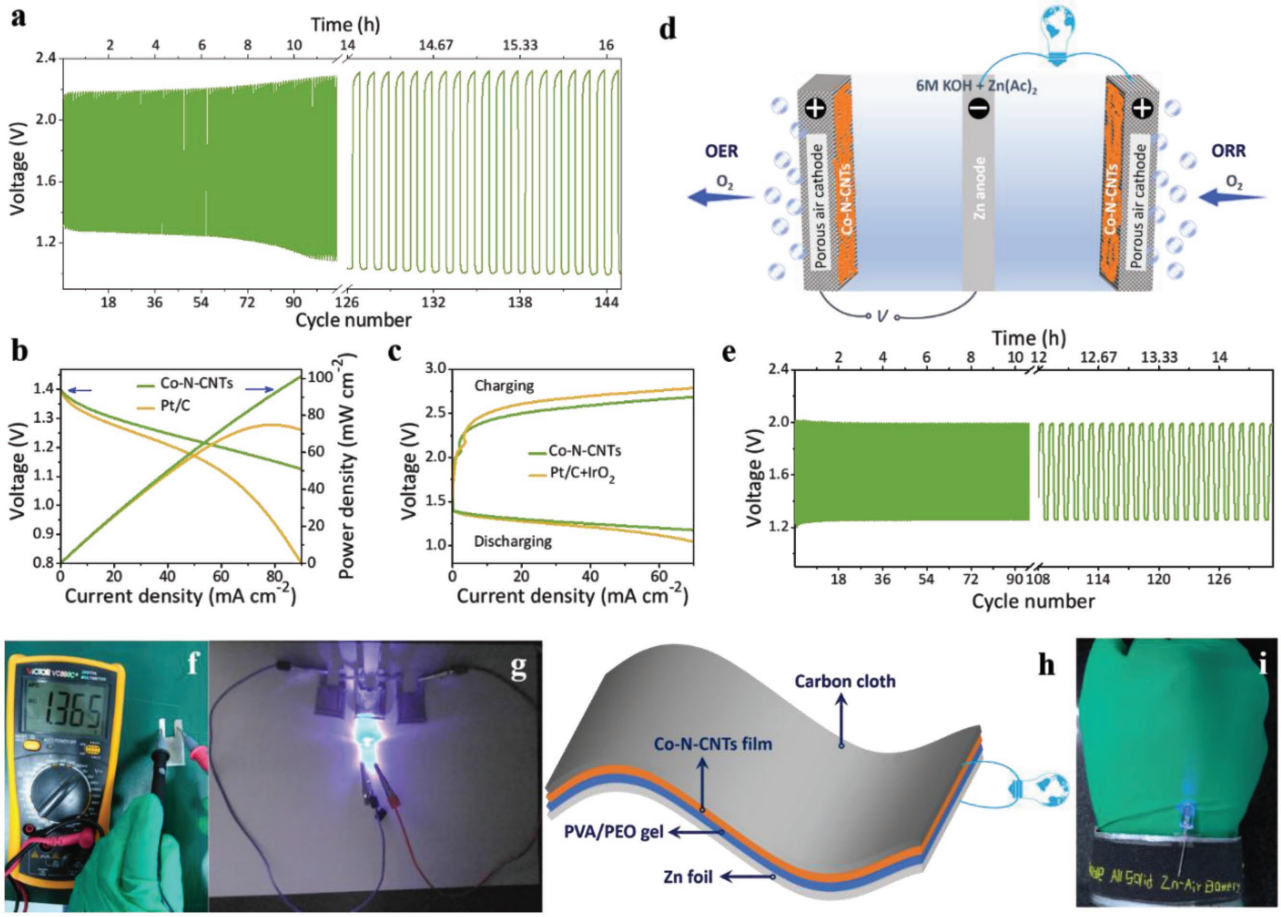

Figure 5. Fabrication and performance of rechargeable Zn–air batteries. a) Galvanostatic discharge–charge cycling curves at 2 mA cm^{-2} of two-electrode rechargeable Zn–air battery with the Co-N-CNT catalyst. b) Polarization and power density curves of primary Zn–air batteries using Pt/C and Co-N-CNTs as ORR catalyst (mass loading of 1 mg cm^{-2}) at a scan rate of 5 mV s^{-1}. c) Schematic of the basic configuration of a three-electrode rechargeable Zn–air battery. d) Charge and discharge polarization curves of three-electrode Zn–air batteries using Co-N-CNT catalyst as both air electrodes, together with the corresponding curve (Pt/C + IrO_2) for the three-electrode Zn–air battery with commercial Pt/C and IrO_2 nanoparticles as each of the air electrodes, respectively. e) Galvanostatic discharge–charge cycling curves of the three-electrode Zn–air battery with the Co-N-CNTs as catalyst at 2 mA cm^{-2}. f) Photograph of the assembled all-solid-state Zn–air battery exhibiting a minimum open circuit voltage of ≈1.365 V measured with a voltammeter. g) Photograph of a lighted green LED (5 mm, ≈3.2 V) powered by three all-solid-state Zn–air batteries interconnected in series. h) Schematic representation and i) photograph of the wearable all-solid-state rechargeable Zn–air battery where a bigger bracelet with three batteries interconnected in series can light a green LED.

© 2017 WILEY-VCH Verlag GmbH & Co. KGaA, Weinheim

and electrolytes to the active sites as well as increasing amount of active sites.[9,18]

In a rechargeable Zn–air battery, the kinetics is mainly limited by the cathode reaction[39]

$$O_2 + 2H_2O + 4e^- \underset{\text{OER}}{\overset{\text{ORR}}{\rightleftharpoons}} 4OH \quad (1)$$

Figure 5c displays the discharge and charge polarization curves for the three-electrode batteries with different air electrodes. Indeed, the Co-N-CNT battery performance significantly enhances by using an optimized three-electrode configuration (Figure 5d), which prevents the bifunctional catalyst from contacting with the oxidative (or reductive) potential during ORR (or OER). The rechargeable Zn–air battery using Co-N-CNTs for the air electrodes shows no obvious voltage change over 130 discharge/charge cycles (for ≈15 h; Figure 5e), which is better than that of a Zn–air battery using Pt/C and IrO_2 as the ORR and OER catalysts, respectively (Figure S25, Supporting Information). As shown in Table S3 (Supporting Information), our battery is better than most of the recently reported rechargeable Zn–air batteries based on carbon-based nanomaterials[40,41] and even metal oxides.[42]

To meet specific energy and/or power needs of various practical applications, multiple Zn–air batteries (Figure S26, Supporting Information) can be integrated into series circuits. As exemplified in Figure 5f, one Zn–air battery using Co-N-CNTs as air electrodes can generate a high open-circuit potential (OCP) of ≈1.365 V (for Pt/C–IrO_2 hybrid air electrodes, OCP is ≈1.208 V; Figure S27, Supporting Information) where it only needs three batteries in series to power blue light-emitting diodes (LEDs; 5 mm, ≈3.2 V) (Figure 5g). To demonstrate potential applications in flexible/wearable optoelectronics, we have further developed flexible all-solid-state Zn–air batteries composed of a Co-N-CNT air-cathode, carbon cloth current collector, zinc foil anode, and alkaline polyvinyl alcohol (PVA) gel electrolyte (Figure 5h). Three all-solid-state flexible Zn–air batteries integrated into a series circuit to assemble a wearable bracelet (Figure 5i) could also be used to power a blue LED under the bending condition.

3. Discussion

Among a handful of reports on Co encapsulated in graphene layers or carbon nanotubes as bifunctional air electrodes (Table S2, Supporting Information), a few have reported such amazing activity and long-term cycling stability as our Co-N-CNTs. These superior results are speculated to originate from the following reasons: (1) A synergetic role of the doped pyridinic and graphitic nitrogen in carbon lattice as well as the encapsulated transition metal nanoparticles stimulates an enhanced intrinsic electrocatalytic activity on the carbon-based multifunctional catalysts;[10,43] (2) Co nanoparticles increase the graphitization degree of surface carbon layer during carbonization,[44] and the surface carbon shells prevent acid leaching, oxidation, and aggregation of Co nanoparticles,[12,45] which promise an excellent durability in the electrocatalytic process and electron transfer to the surface; (3) the strong coordination structure between cobalt and nitrogen atoms could also play a key role on the activity and stability of the Co-N-CNTs.[12,46]

4. Conclusion

In summary, we have developed a facile, low-cost, and scalable approach to prepare Co-N-CNTs by pyrolyzing 2D leaf-like ZIF-L. The resultant Co-N-CNTs show ultrahigh catalytic activities for both ORR and OER and demonstrate to be excellent bifunctional air electrodes for primary and rechargeable Zn–air batteries. Typically, our primary batteries based on the Co-N-CNT air electrode operating in ambient air with an aqueous KOH electrolyte exhibited a high OCP of 1.365 V, current density of ≈90 mA cm^{-2}, and a peak power density of ≈101 mW cm^{-2}. A three-electrode rechargeable battery using two Co-N-CNT air electrodes to separate ORR and OER shows good stability (130 cycles for 15 h of operation). Our study underlines the great potential of Co-N-CNTs as bifunctional air electrodes and the advantages of 2D ZIF-L as the single precursor to prepare these materials. We anticipate that our nanomaterial will also be useful for other cutting-edge applications.

5. Experimental Section

Synthesis of Co/Zn (1:1) ZIF-L: The synthesis procedure of Co/Zn (1:1) ZIF-L was similar to Zn ZIF-L. $Zn(NO_3)_2{\cdot}6H_2O$ and $Co(NO_3)_2{\cdot}6H_2O$ were dissolved in 40 mL of DI water with the molar ratios of Zn^{2+}/Co^{2+} = 1:1, and then 2-mIm was added to the same amount of DI water. Details are presented in Table S1 (Supporting Information).

Synthesis of Co-N-CNTs: Co-N-CNTs were obtained by means of a simple one-step pyrolysis method. In a typical process, 500 mg Co/Zn (1:1) ZIF-L was heated to 900 °C at a rate of 5 °C min^{-1} in a tube furnace under Ar atmosphere and maintained at this temperature for 2 h. Subsequently, the heating system is naturally cooled to the room temperature. The final product is Co-N-CNTs.

Preparation of the Working Electrode: The catalyst ink was prepared by ultrasonically dispersing 10.0 mg samples in the mixture of 900 µL isopropanol, 80 µL deionized water (18 MΩ cm^{-1}), and 20 µL dilute aqueous Nafion solution (5 wt% solution in a mixture of lower aliphatic alcohols and DuPont water). The working electrode was obtained by ultrasonically dispersing and dropping 20 µL catalyst ink on a glassy-carbon RRDE (disk area: 0.2475 cm^2; ring area: 0.1866 cm^2) from Pine Instruments. The catalyst loading was all 0.81 mg cm^{-2} based on the geometric electrode area of 0.2475 cm^2.

Electrochemical Evaluations: A three-electrode cell was used to do the electrochemical measurements. Hg/HgO for alkaline electrolyte and Ag/AgCl (3 M Cl^-) for acid environment were used as reference electrodes, respectively. The Pt wire was used as a counterelectrode. All electrochemical measurements were carried out at 25 °C. ORR/OER evaluation was performed in electrolyte saturated and protected by bubbling O_2 with a flow of 20 sccm. The scan rate for ORR/OER measurements was 5 mV s^{-1}. The ORR polarization curves were collected at various rotation rates ranging from 625 to 2025 rpm for calculating the transferring electron number. The accelerated durability tests were performed at room temperature in oxygen saturated 0.1 M KOH solution at a sweep rate of 50 mV s^{-1} for 10 000 cycles. The *i–t* chronoamperometric response was conducted in oxygen saturated 0.1 M KOH solution at 0.8 V versus RHE for 5 h.

The steady-state *i–t* chronoamperometric response was tested at the polarizing potential of 0.8 V versus RHE in the O_2-saturated electrolyte, and 10% (v/v) CO or 3 mol methanol was introduced into the 500 mL electrolyte at 33 or 40 s to examine the CO poisoning and methanol crossover, respectively. For comparison, the commercial Pt/C catalyst

© 2017 WILEY-VCH Verlag GmbH & Co. KGaA, Weinheim

with Pt loading of 20 wt% (Johnson Matthey, Pt particle size: 2–5 nm) and IrO_2 were also used as the benchmarking catalysts for ORR and OER respectively, and the same procedure as described above was used to conduct the electrochemical measurement, and the Pt loadings was 20 μg_{Pt} cm^{-2} for the commercial Pt/C catalyst.

Zinc–Air Battery Tests: The measurements of rechargeable zinc–air batteries were performed on home-built electrochemical cells. All data were collected from the as-fabricated cell with a CHI 760D (CH Instruments, Inc., Shanghai, China) electrochemical workstation at room temperature. Briefly, zinc foil was used as anode and catalysts loaded on the 1 cm × 2 cm carbon paper (catalyst loading amount of 1.0 mg cm^{-2}) was used as the air cathode. For comparison, the rechargeable battery was also made from a mixture of Pt/C and IrO_2 with a mass ratio of 1:1. The electrolyte was the mixture solution of 6.0 M KOH and 0.2 M zinc acetate.

The all solid-state Zn–air battery was fabricated by a polished zinc foil as anode, catalyst as cathode, gel polymer as solid electrolyte, and carbon cloth as charge collector. The solid electrolyte was prepared as follow: 1 g PVA powder (1788-PVA/1799-PVA = 2:1) was added to 10 mL H_2O at room temperature under stirring for 45 min and then heated up to 95 °C. After the solution was transferred into transparent gel, 1 mL 18 M KOH was added to the mixture. After being stirred for 0.5 h, the gel was poured onto a glass plate and freezed in a freezer at –20 °C for 2 h and then transferred to 0 °C for 4 h. The procedure was obtained after thawing at room temperature. For 1788-PVA, the better swelling and stretch properties can enhance ionic conductivity, and 1799-PVA supports the main morphology of gel.

Supporting Information

Supporting Information is available from the Wiley Online Library or from the author.

Acknowledgements

T.T.W. and Z.K.K. contributed equally to this work. The authors acknowledge support from the National Key Research and Development Program of China (Grant No. 2016YFA0202603) and the National Natural Scientific Foundation of China (NSFC) through Grant Nos. 51372186, 516722040, and 21502146. F.V. appreciates the financial support from Tomsk Polytechnic University Competitiveness Enhancement Program grant (VIU-316/2017). The authors also wish to thank Prof. Xiaoqing Liu and Xiaoxing Ke for TEM analytical measurements performed at JEM-2100F in the Materials Analysis Center of Wuhan University of Technology.

Conflict of Interest

The authors declare no conflict of interest.

Keywords

2D and leaf-like zeolitic imidazolate frameworks, bifunctional air electrodes, cobalt–nitrogen–carbon nanotubes, rechargeable zinc–air batteries

Received: September 1, 2017
Revised: October 7, 2017
Published online: December 4, 2017

[1] J. F. Parker, C. N. Chervin, I. R. Pala, M. Machler, M. F. Burz, J. W. Long, D. R. Rolison, *Science* **2017**, *356*, 415.
[2] M. Armand, J. M. Tarascon, *Nature* **2008**, *451*, 652.
[3] C. Y. Su, H. Cheng, W. Li, Z. Q. Liu, N. Li, Z. Hou, F. Q. Bai, H. X. Zhang, T. Y. Ma, *Adv. Energy Mater.* **2017**, *7*, 1602420.
[4] Y. Li, M. Gong, Y. Liang, J. Feng, J. E. Kim, H. Wang, G. Hong, B. Zhang, H. Dai, *Nat. Commun.* **2013**, *4*, 1805.
[5] Y. Su, Z. Yao, F. Zhang, H. Wang, Z. Mics, E. Cánovas, M. Bonn, X. Zhuang, X. Feng, *Adv. Funct. Mater.* **2016**, *26*, 5893.
[6] Z. Liu, H. Cheng, N. Li, T. Ma, Y. Su, *Adv. Mater.* **2016**, *28*, 3777.
[7] H. Cheng, M. Li, C. Su, N. Li, Z. Liu, *Adv. Funct. Mater.* **2017**, *27*, 1701833.
[8] Y. Li, H. Dai, *Chem. Soc. Rev.* **2014**, *43*, 5257.
[9] M. Zeng, Y. Liu, F. Zhao, K. Nie, N. Han, X. Wang, W. Huang, X. Song, J. Zhong, Y. Li, *Adv. Funct. Mater.* **2016**, *26*, 4397.
[10] D. Deng, L. Yu, X. Chen, G. Wang, L. Jin, X. Pan, J. Deng, G. Sun, X. Bao, *Angew. Chem., Int. Ed.* **2013**, *52*, 371.
[11] X. Cui, P. Ren, D. Deng, J. Deng, X. Bao, *Energy Environ. Sci.* **2016**, *9*, 123.
[12] J. Wang, D. Gao, G. Wang, S. Miao, H. Wu, J. Li, X. Bao, *J. Mater. Chem. A* **2014**, *2*, 20067.
[13] Z. K. Kou, K. Cheng, W. Hui, R. Sun, B. B. Guo, S. C. Mu, *ACS Appl. Mater. Interfaces* **2016**, *8*, 3940.
[14] Z. Wang, S. Peng, Y. Hu, L. Li, T. Yan, G. Yang, D. Ji, M. Srinivasan, Z. Pan, S. Ramakrishna, *J. Mater. Chem. A* **2017**, *5*, 4949.
[15] X. Cai, B. Y. Xia, J. Franklin, B. Li, X. Wang, Z. Wang, L. Chen, J. Lin, L. Lai, Z. Shen, *J. Mater. Chem. A* **2017**, *5*, 2488.
[16] X. Han, X. Wu, C. Zhong, Y. Deng, N. Zhao, W. Hu, *Nano Energy* **2017**, *31*, 541.
[17] D. P. He, Y. L. Xiong, J. L. Yang, X. Chen, Z. X. Deng, M. Pan, Y. Li, S. C. Mu, *J. Mater. Chem. A* **2015**, *5*, 1930.
[18] J. Wang, H. Wu, D. Gao, S. Miao, G. Wang, X. Bao, *Nano Energy* **2015**, *13*, 387.
[19] B. Guan, Y. U. Le, X. W. Lou, *Energy Environ. Sci.* **2016**, *9*, 3092.
[20] B. Y. Xia, Y. Yan, N. Li, H. B. Wu, X. W. Lou, X. A. Wang, *Nat. Energy* **2016**, *1*, 15006.
[21] M. Kuang, Q. Wang, P. Han, G. Zheng, *Adv. Energy Mater.* **2017**, *7*, 1700193.
[22] R. Chen, J. Yao, Q. Gu, S. Smeets, C. Baerlocher, H. Gu, D. Zhu, W. Morris, O. M. Yaghi, H. Wang, *Chem. Commun.* **2013**, *49*, 9500.
[23] T. Palaniselvam, V. Kashyap, S. N. Bhange, J. B. Baek, S. Kurungot, *Adv. Funct. Mater.* **2016**, *26*, 2150.
[24] Z. K. Kou, T. Meng, B. B. Guo, I. S. Amiinu, W. Li, J. Zhang, S. Mu, *Adv. Funct. Mater.* **2017**, *27*, 1604904.
[25] S. Gao, Y. Lin, X. Jiao, Y. Sun, Q. Luo, W. Zhang, D. Li, J. Yang, Y. Xie, *Nature* **2016**, *529*, 68.
[26] P. Matousek, N. Stone, *Chem. Soc. Rev.* **2016**, *45*, 1794.
[27] Z. K. Kou, B. B. Guo, Y. F. Zhao, S. F. Huang, T. Meng, J. Zhang, W. Q. Li, I. S. Amiinu, Z. H. Pu, M. Wang, M. Jiang, X. Liu, Y. Tang, S. C. Mu, *ACS Appl. Mater. Interfaces* **2017**, *9*, 3702.
[28] J. Zhang, C. Y. Zhang, Y. F. Zhao, I. S. Amiinu, H. Zhou, X. B. Liu, Y. F. Tang, S. C. Mu, *Appl. Catal., B* **2017**, *211*, 148.
[29] Y. Z. Chen, C. Wang, Z. Y. Wu, Y. Xiong, Q. Xu, S. H. Yu, H. L. Jiang, *Adv. Mater.* **2015**, *27*, 5010.
[30] K. Gong, F. Du, Z. Xia, M. Durstock, L. Dai, *Science* **2009**, *323*, 760.
[31] A. Aijaz, J. Masa, C. Rösler, W. Xia, P. Weide, R. A. Fischer, W. Schuhmann, M. Muhler, *ChemElectroChem* **2016**, *4*, 188.
[32] P. Yin, T. Yao, Y. Wu, L. Zheng, Y. Lin, W. Liu, H. Ju, J. Zhu, X. Hong, Z. Deng, *Angew. Chem., Int. Ed.* **2016**, *55*, 10800.
[33] J. Liu, M. Zheng, X. Shi, H. Zeng, H. Xia, *Adv. Funct. Mater.* **2016**, *26*, 919.
[34] Z. Q. Liu, H. Cheng, N. Li, T. Y. Ma, Y. Z. Su, *Adv. Mater.* **2016**, *28*, 3777.
[35] A. Holewinski, S. Linic, *J. Electrochem. Soc.* **2012**, *159*, H864.
[36] J. Fu, Z. P. Cano, M. G. Yu, A. Park, M. Fowler, Z. Chen, *Adv. Mater.* **2016**, *29*, 1604685.

© 2017 WILEY-VCH Verlag GmbH & Co. KGaA, Weinheim

[37] G. Fu, Y. Chen, Z. Cui, Y. Li, W. Zhou, S. Xin, Y. Tang, J. B. Goodenough, *Nano Lett.* **2016**, *16*, 6516.
[38] Li, G. Wang , X. Fu, J. Li, J. Park, M. G. Zhang, Y. G. Lui, Z. Chen, *Angew. Chem., Int. Ed.* **2016**, *55*, 4977.
[39] A. Kraytsberg, Y. Ein-Eli, *Nano Energy* **2013**, *2*, 468.
[40] J. Zhang, Z. Zhao, Z. Xia, L. Dai, *Nat. Nanotechnol.* **2015**, *10*, 444.
[41] H. B. Yang, J. Miao, S. F. Hung, J. Chen, H. B. Tao, X. Wang, L. Zhang, R. Chen, J. Gao, H. M. Chen, *Sci. Adv.* **2016**, *2*, e1501122.
[42] G. Du, X. Liu, Y. Zong, T. S. Hor, A. Yu, Z. Liu, *Nanoscale* **2013**, *5*, 4657.
[43] J. Deng, L. Yu, D. Deng, X. Chen, F. Yang, X. Bao, *J. Mater. Chem. A* **2013**, *1*, 14868.
[44] L. Jiang, J. Yan, L. Hao, R. Xue, G. Sun, B. Yi, *Carbon* **2013**, *56*, 146.
[45] G. Zhang, C. Li, J. Liu, L. Zhou, R. Liu, X. Han, H. Hu, H. Huang, Y. Liu, Z. Kang, *J. Mater. Chem. A* **2014**, *2*, 8184.
[46] H. W. Liang, W. Wei, Z. S. Wu, X. Feng, K. Müllen, *J. Am. Chem. Soc.* **2013**, *135*, 16002.

© 2017 WILEY-VCH Verlag GmbH & Co. KGaA, Weinheim